Korean J. Chem. Eng., 40(5), 1234-1239 (2023)
DOI: 10.1007/s11814-022-1359-x

pISSN: 0256-1115
eISSN: 1975-7220

The electrochemical performance of lotus-root shaped meso-/macroporous TiO_2 anode for lithium-ion battery

Sun-gie Han*, Minsun Park, Seong Huh**,†, and Yong Sun Won*,†**

*Department of Chemical Engineering, Pukyong National University, Busan 48513, Korea
**Department of Chemistry and Protein Research Center for Bio-Industry,
Hankuk University of Foreign Studies, Yongin 17035, Korea
(*Received 11 August 2022 • Revised 17 November 2022 • Accepted 28 November 2022*)

Abstract−As an alternative to the graphite-based anode in lithium-ion battery (LIBs), the TiO_2-based anode has continuously drawn attention due to its high stability and long operating life, especially in the field of electric vehicles (EVs). Although a spinel structure lithium titanate (LTO, $Li_4Ti_5O_{12}$) anode is commercially available, there has been a constant need to improve the anode capacity with TiO_2-based materials because they have much higher theoretical capacity compared to LTO. In this regard, nanostructured TiO_2-based materials with high surface area are thought to be ideal for LIB anode application. In this study, a lotus-root shaped meso-/macroporous TiO_2 (LR-700) material was prepared and employed as an anode material for LIB with expectancy to have large channels for easy Li^+ insertion and thus show better electrical property. Coin cell tests were carried out with the anodes prepared from LR-700, LTO, and nano-sized TiO_2 powder (known as P25) for comparison by charging and discharging at 0.5 C. Despite the presence of large macroporous channels and mesopores in the walls for LR-700, the capacity of 158 mAh/g for LR-700 anode was found to be slightly lower than the LTO's theoretical discharge capacity of 175 mAh/g. We envision that less thicker walls would enhance the performance through effective ion diffusion and electronic conduction.

Keywords: Titania, Lithium-ion Battery, Anode Materials, Mesoporous Materials, Porous Materials

INTRODUCTION

Owing to the tremendous increase of various applications, such as portable electronic devices and energy storage systems (ESS), the need for lithium-ion batteries (LIBs) with excellent performance has exploded as well [1]. In particular, the current spread of electric vehicles (EVs) does not only demand the capacity of batteries, but also the stability and operating life, or long-term cyclability, of rechargeable batteries. In this regard, new stable anode materials for LIBs with superior performance have been sought in the past decades [2]. The graphite anode for LIBs is known to have excellent capacity (372 mAh/g), well compatible with the lithium cobalt oxide ($LiCoO_2$, LCO) cathode [3]. To increase the capacity of batteries, there have been numerous researches on the silicon-based anode having a very large capacity of 4,200 mAh/g [4,5]. However, the volume expansion was very severe during the lithium alloying and dealloying and thus long operation life is hardly guaranteed [6,7]. Although the graphite anode has a decent operation life, it would not be sufficient for EVs and the graphite anode does not go with the cheap lithium manganese oxide ($LiMn_2O_4$, LMO) cathode due to severe capacity decrease followed by manganese (Mn) dissolution [8]. On the contrary, titanium (Ti)-based anode materials have a very low volumetric expansion rate with their structural stability, and thus can be operated for a long time, being robust to the Mn dissolution [9,10]. For example, although lithium titanate ($Li_4Ti_5O_{12}$, LTO) with a spinel structure is commercially available, it has a limited theoretical discharge capacity of 175 mAh/g, less than the half of the graphite's [11,12]. Moreover, the structural stability of Ti-based anodes comes with a lower open circuit voltage (V_{oc}) of 1.62 V, compared to 2.0 V of the graphite [13].

Therefore, there have been intense research efforts to use TiO_2 as an alternative to LTO because it has a large theoretical capacity of 336 mAh/g (one Li^+ ion per TiO_2), close to that of the graphite [14]. Generally, TiO_2 anode is structurally very stable, environmentally benign, and cost-effective. Several polymorphs of TiO_2 have been investigated for LIBs [15]. Both anatase and TiO_2(B) with monoclinic phase have been considered as the most promising anode materials among other polymorphs due to their fast Li^+ insertion/deinsertion [16]. Various TiO_2 materials with mesoscale porosity have been being tested to overcome the low ionic or electrical conductivity and the shallow Ti diffusion into a bulk shape of TiO_2 [17-21]. Porous anatase TiO_2 anode has been known for its stable cyclability with a constant operating potential [16]. The low volume expansion (<4%) during Li^+ charge/discharge process is another merit for LIBs [15]. Several 3D and 2D structures of TiO_2 materials were also tested as an anode for LIBs. Generally, porous 3D TiO_2 structures are thought to be more ideal than 1D or 2D structures due to effective ion transport and better electronic conductivity. For example, the hierarchical mesoporous TiO_2 spheres showed a capacity of 181 mAh/g after 100 cycles [18]. MTNHTS (mesoporous TiO_2 hierarchical tubular superstructure) also displayed a high capacity of 210 mAh/g at 1 C [20]. The 3D mesoporous anatase TiO_2 nano-

†To whom correspondence should be addressed.
E-mail: shuh@hufs.ac.kr, yswon@pknu.ac.kr

crystals of BET surface area of 258 m^2/g showed capacity of 158-163 and 96-110 mAh/g at rates of C/10 and 1 C, respectively [15]. Hierarchically structured mesoporous anatase TiO_2 microspheres also showed a capacity as high as 210 mAh/g [22]. Thick TiO_2 films with vertically oriented large mesopores (7-9 nm) exhibited a remarkably high capacity of 254 mAh/g after 200 cycles at C/3 rate. The reason for this exceptional capacity (76% of the theoretical value) was attributed to short Li^+ diffusion length together with high surface area [23]. Contrarily, 2D anatase TiO_2 nanosheets (thickness ~10 nm) displayed a capacity of 150 mAh/g [24]. TiO_2 hollow spheres also exhibited a very similar capacity of 148 mAh/g [25]. Petal-like TiO_2 nanosheets showed enhanced capacity of 180 mAh/g [26]. Mesoporous single-grain layer of anatase TiO_2 nanosheets showed very stable operation up to 4,000 cycles of charge/discharge with a relatively low capacity of 73 mAh/g [27].

Recently, we prepared unique lotus-root shaped meso-/macroporous TiO_2 (LR-TiO_2) materials with hierarchical porosity and applied LR-700 (LR-TiO_2 heat-treated at 700 °C) to the photo-electrode of dye-sensitized solar cells (DSSCs) [28]. The phase of LR-700 is mainly anatase with a very small portion of rutile. Interestingly, the longitudinal macroporous channels of LR-700 rendered the supply and withdrawal of electrolyte ions more efficiently to improve the performance of DSSCs with increased photo-current. Based on these results, we envision that LR-700 can be a good anode material for LIBs due to its unique hierarchical bimodal pore structure. In this study, we applied the LR-700 to the anode of LIBs and compared its performance (capacity and capacity retention) to those of LTO and nano-sized P25 anodes. By using electrical impedance spectroscopy (EIS) data, equivalent circuits were constructed for more detailed analysis.

EXPERIMENTAL

1. Preparation of LR-700 TiO_2

LR-700 TiO_2 material was prepared according to our previous literature method using cetyltrimethylammonium hydroxide (CTAOH) template [28].

2. Preparation of Coin Cells

TiO_2 electrode for coin cell tests was prepared by casting the slurry containing 80 wt% LR-700 (or LTO and P25), 10 wt% carbon black (Super PTM Conductive, 99%, Alfa Aesar, USA) and 6 wt% carboxymethyl cellulose (CMC)/4 wt% styrene-butadiene rubber (SBR) in Di-water on Cu foil. The slurry was applied onto the Cu foil uniformly to a thickness of 140 μm. It was dried at 150 °C in vacuum for 12 h and the coated Cu foil was placed between two steel plates and pressed. And then, it was designed to have material loading of ~1.73 mg/cm^2. The tested cells had a typical three-electrode construction using lithium foils as both the counter and reference electrodes, Celgard 2400 microporous membrane as separator, and 1 M $LiPF_6$ dissolved in ethylene carbonate (EC), dimethyl carbonate (DMC), and ethyl methyl carbonate (EMC) (1 : 1 : 1, v/v/v) as the electrolyte. CR2032 coin half-cells were assembled in an argon-filled glove box.

3. Measurements

SEM (S-2400, TESCAN (Czech), VEGA II LSU), and gas sorption analyzer (Quantachrome autosorb-iQ) were used to characterize LR-700 TiO_2 and P25 powder. The coin half-cells were galvanostatically discharged to 0.01 V and charged to 3.0 V at a C/5 rate using a cycler (WBCS300L, WonAtech Co., Korea). Electrochemical impedance spectroscopy (EIS) was performed using an impedance analyzer (ZIVE SP1, WonAtech Co., Korea) after charging at a C/5 rate to 3.0 V or discharging at a C/5 rate to 0.1 V. EIS measurements were carried out using a 30 mV of amplitude in the frequency range of 0.1 Hz to 100 kHz.

RESULTS AND DISCUSSION

To characterize the performance of LR-700 as an anode for LIB, standard coin cells were fabricated and tested. LTO and P25 were similarly investigated as reference samples. LTO and P25 are Ti-based powder with very small particle sizes of ~200 nm and ~21 nm, respectively. LTO can be considered as a promising alternative anode material for graphite due to its three-dimensional (3D) channel structure ideal for Li^+ transport [29]. Ohzuku et al. noted that substantial chemical changes of LIBs made of LTO occurred during the transition between the two phases of the Li-rich phase (rock-salt-LTO) and Li-deficient phase (spinel-LTO) [30]. Despite this change, the corresponding volume change was reported to be only 0.2-0.3%. Due to the negligible volume change, this type of material is called a zero-strain insertion material, exhibiting excellent reversibility as an anode for LIBs. During the two-phase transition from spinel-LTO to rock-salt-LTO, three Ti^{4+} are reduced to Ti^{3+}. The corresponding electrochemical reaction can be described as follows:

$$Li_4Ti_5O_{12}\ (\text{spinel-LTO}) + 3Li^+ + 3e^- \leftrightarrow Li_7Ti_5O_{12}\ (\text{rock-salt-LTO}) \quad (1)$$

As seen from Eq. (1), the amount of Li^+ per weight is small, equivalent to the theoretical capacity of 175 mAh/g. On the other hand, the half-cell reaction formula between TiO_2 and Li^+ is written differently as follows:

$$TiO_2 + xLi^+ + xe^- \rightarrow Li_xTiO_2\ (x \leq 1) \quad (2)$$

The amount of lithium ions that TiO_2 reacts per unit weight is larger than that of LTO, equivalent to the theoretical capacity of 336 mAh/g [14,15,31]. It was revealed that tetragonal anatase TiO_2 showed the maximum reversible Li^+ insertion at x=0.5, resulting in orthorhombic $Li_{0.5}TiO_2$, and the corresponding capacity was 168 mAh/g [14]. Further Li^+ insertion process becomes sluggish at x>0.5. Thus, the theoretical capacity is hardly reached, mainly due to the active surface area and pore size limitations. Accordingly, nanostructured porous TiO_2 materials having high surface areas with suitable pore dimensions and particle sizes are thought to be ideal anodes for high capacity [18-21]. Sufficiently large pore dimensions also render the movements of ions more freely and the performance of LIBs can be significantly improved.

Fig. 1 shows particle morphologies of LR-700 and nanocrystalline P25 samples characterized by scanning electron microscopy (SEM). The featured difference is that LR-700 has longitudinal large macropores with diameters of ~1 μm which can behave as effective reservoirs for ions. Meanwhile, the Brunauer-Emmett-Teller (BET) surface area of P25 is two-fold larger than that of LR-700 by cryogenic nitrogen gas sorption measurements: 49 and 27 m^2/g,

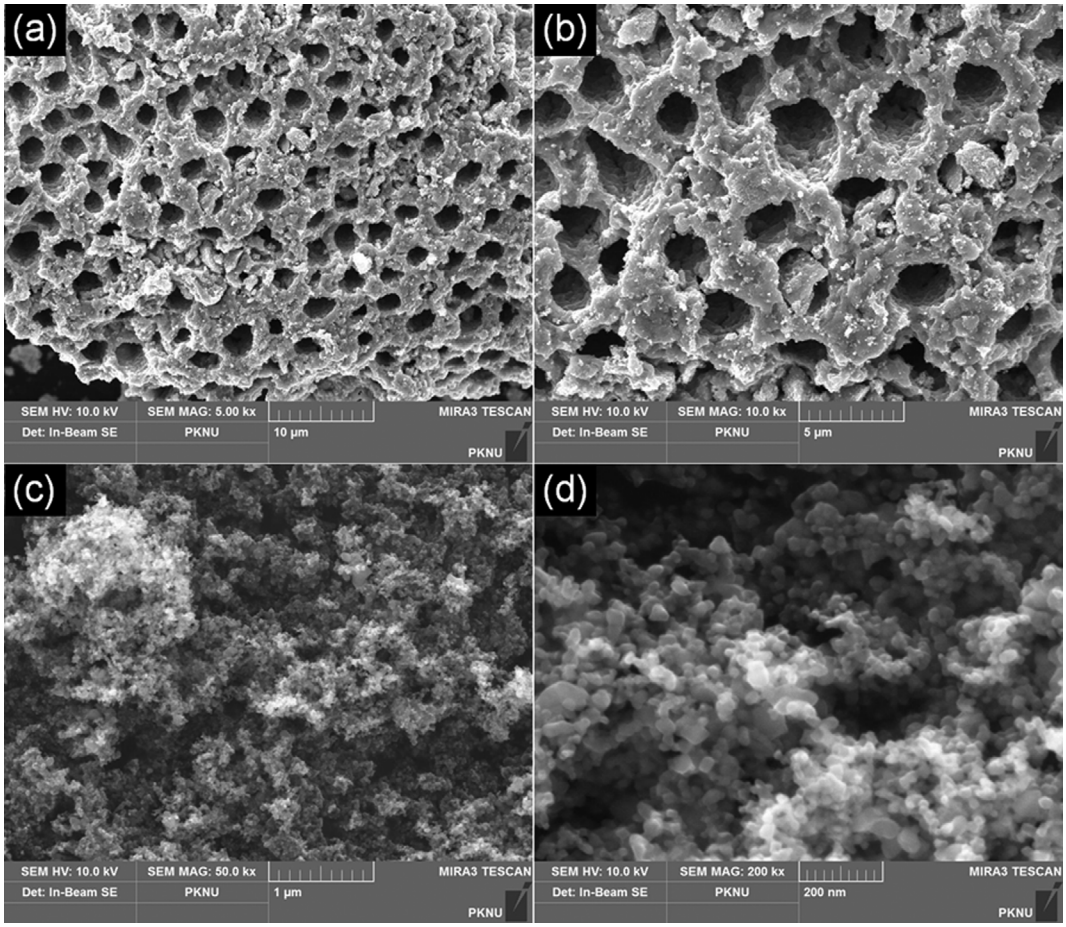

Fig. 1. SEM images of LR-700 (a), (b) and P25 (c), (d) at different magnification.

respectively [28]. Meso-/macroporous LR-700 showed bimodal porosity with mesopores (28.3 nm) and randomly distributed macropores (*ca.* 1-3 μm). Considering that Li^+ is inserted into the TiO_2 surface, the capacity of LIBs with P25 is expected to be higher than LR-700: the larger the surface area, the more reactive Li^+. Nonetheless, the results showed the opposite trend, as given in Fig. 2 and Table 1. The capacity of LR-700 after the 50th cycle is above threefold larger than that of P25; 158 mAh/g and 45 mAh/g, respectively. It suggests that the surface area of P25 was not effectively used for the reaction with Li^+. Similar to our previous results with DSSCs [28], very small pores were formed between P25 nanoparticles and it was very hard for Li^+ dissolved in the electrolyte to penetrate deep into the interior. Thus, the surface area in the deep interior portion did not contribute effectively to the Li^+ insertion. The resistance thus increases as Li^+ moves deeper from the surface to the unreacted interior. However, bimodal meso-/macroporous LR-700 has many longitudinal macroporous channels to convey Li^+ to the interior surfaces more easily with much less resistance. Although the specific capacity of LR-700 is lower than the theoretical capac-

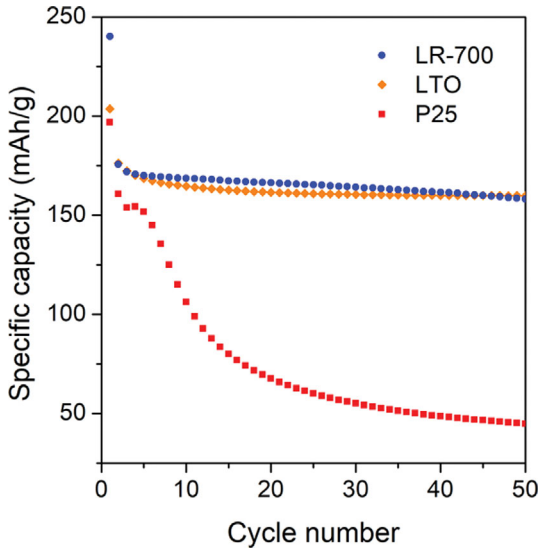

Fig. 2. Lithium-ion battery cycling performances of LR-700, LTO, and P25 anodes up to 50 cycles at 0.5 C rate.

Table 1. The specific capacity and capacity retention of TiO_2 anodes

	LR-700	LTO	P25
1st cycle capacity (mAh/g)	240	204	197
50th cycle capacity (mAh/g)	158	160	45
Retention rate (%)	66	78	23

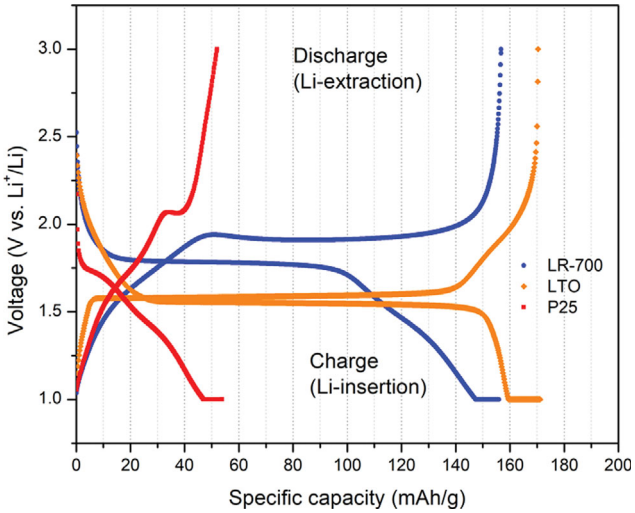

Fig. 3. Galvanostatic discharge-charge curves vs. Li/Li^+ for LR-700, LTO, and P25 after 25th cycle at a rate of 0.2 C. The voltage range is from 1.0 to 3.0 V.

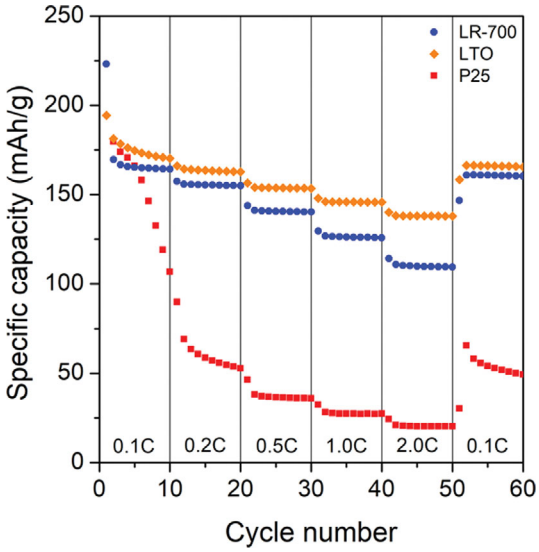

Fig. 4. The potential-capacity profiles of three TiO_2 anodes upon changing current rate (0.1 C→0.2 C→0.5 C→1.0 C→2.0 C→0.1 C) every 10 cycle. All measurements were conducted in the voltage range 1-3 V.

Table 2. The C-rate dependent performances of TiO_2 anodes

C-rate	Cycle	Capacity (mAh/g)		
		LR-700	LTO	P25
0.1	10th	164	170	107
0.2	20th	155	163	53
0.5	30th	140	153	36
1.0	40th	126	146	27
2.0	50th	109	138	20
0.1	60th	160	166	49

ity of TiO_2 (336 mAh/g), it is quite comparable to LTO, which has the specific capacity of 160 mAh/g after 50 cycles. However, the retention rate for LR-700 (66%) is smaller than that of LTO (78%). The retention rate for LR-700 is much larger than that of P25 (23%). The specific capacity of LR-700 anode is closely similar to 2D anatase TiO_2 nanosheets and TiO_2 hollow spheres [24,25].

The three TiO_2 anode materials were compared more in detail by analyzing the discharge (Li^+ insertion)-charge (Li^+ extraction) curves of the TiO_2 electrodes after 25th cycle, as depicted in Fig. 3. LTO displays a typical ultraflat biphasic transition voltage plateau for discharge (Li^+ insertion) process at around 1.55 V vs. Li/Li^+ and the plateau for charge (Li^+ extraction) process at 1.60 V [29,32]. Constant voltage was maintained over these discharge-charge processes, indicating low polarization effect and good reaction kinetics [29]. LR-700 showed a similar biphasic plateau after initial monotonic voltage drop (~0.77 V) from the open circuit voltage for discharge process. This biphasic (Li-poor phase and Li-rich phase) process is like the known anatase TiO_2 anode [14,22]. Interestingly, LR-700 showed a biphasic transition plateau at higher voltage for charge process (1.91-1.94 V) with a specific capacity range 48-128 mAh/g. LR-700 showed slightly less efficient Li^+ extraction compared to LTO. This phenomenon can be attributed to the thick TiO_2 walls despite the hierarchical meso-/macroporous pore structure of LR-700. P25 indicates much poorer performance compared to both LTO and LR-700.

The rate dependent performance of the three TiO_2 anodes was also investigated by measuring capacity under varying rate conditions as shown in Fig. 4 and Table 2. All TiO_2 samples showed gradual decrease of the capacity upon the increase of the charge-discharge rate from 0.1 C to 2.0 C. LR-700 showed slightly smaller capacity under the tested rates compared to LTO at 0.1 C, 0.2 C, and 0.5 C. The capacity differences between LR-700 and LTO became larger at high rates of 1.0 C and 2.0 C. This indicates LR-700 is less effective to maintain its capacity at high rates than LTO. Despite the presence of both large macropore and mesopore in the walls, Li^+ cannot insert substantially into the deeper part of the TiO_2 walls of LR-700 due to its thick wall structure. Nonetheless, both LR-700 and LTO exhibited specific capacity (160 and 166 mAh/g) very close to their original values at the rate of 0.1 C (164 and 170 mAh/g) when the rate was changed down to 0.1 C again. Thus, the cycling stability of LR-700 seems to be good like LTO. Interestingly, the capacity of LR-700 is only marginally different from LTO at 0.1 C.

To compare the performance of the three TiO_2 anodes more in detail, each anode was investigated by AC impedance spectroscopy. The EIS data of LIBs were measured after being charged to 3 V. The Nyquist plots were fitted by using ZView program (ver. 3.0) as shown in Fig. 5(a). The corresponding modified Randles equivalent circuits for the three samples are shown in Fig. 5(b)-5(d). All figures of merit indicated by χ^2 values were satisfactorily low. In most of the voltage range, the Nyquist plots are composed of two partially overlapping semicircles at high frequency and midfrequency regions and a straight slopping line at low frequency end, as shown in Fig. 5(a). This curve profile is typical of the electrochemical reaction associated with Li^+ intercalation [33-36]. The first semicircle is rooted in the formation of surface film (R_{sf}), or solid electrolyte interface (SEI), on TiO_2 anode. The second semi-

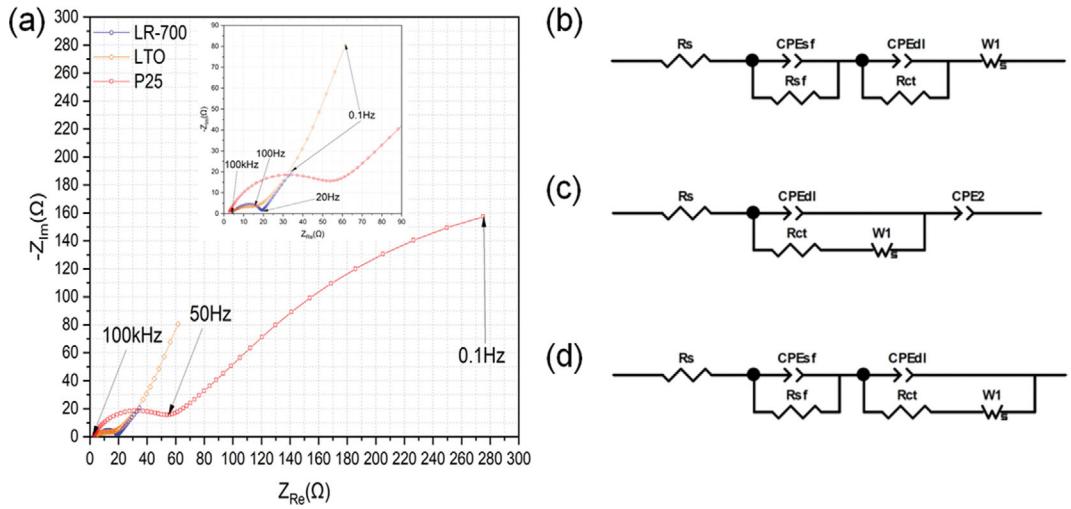

Fig. 5. Nyquist plots of batteries made of LR-700, LTO, and P25 (a). The fitted lines are obtained from the corresponding equivalent circuits of LR-700 (b), LTO (c), and P25 (d). The corresponding χ^2 values are 3.37×10^{-5} (LR-700), 9.15×10^{-5} (LTO), and 1.18×10^{-4} (P25). R_s, R_{sf}, and R_{ct} are the ohmic, surface film, and charge transfer resistances, respectively. CPEs are the constant phase elements describing nonhomogeneous behavior of electrodes and *W* describes the solid state diffusion process inside the TiO_2 particles.

circle is thought to be from the charge transfer between the SEI layer and TiO_2 anode (R_{ct}). The sum of these two resistances is often called an overall impedance [37]. Thus, the overall impedance represents the resistance of Li^+ migration through the SEI film and the charge transfer at the SEI. The overall impedance and the ohmic resistance (R_s) are considered as an intrinsic resistance of the corresponding anode. The R_s stems from the electrical contacts of electrodes and electrolyte, and other cell components. The impedance of Li^+ diffusion in the solid state is responsible for the straight line, also known as the Warburg impedance (Z_w). Therefore, impedance plots generally represent the resistance of the electrolyte at high frequency, the interface at medium frequency, and ion at low frequency [11]. The resistance data for the three TiO_2 anodes are summarized in Table 3. The ohmic resistances (real parts of the impedance) are almost similar, 3.83, 3.12, and 2.47 Ω for LR-700, LTO, and P25, respectively. These small R_s values indicate that the cells were properly assembled. Because all test cells used the same lithium metal as the counter and reference electrode and the same electrolyte, the resistance difference mainly arises at the anode and electrolyte interfaces. Thus, the difference in the graphs (see Fig. 5(a)) mainly comes from the different resistance at the interface between the electrolyte and the anode. As mentioned, the easy supply and withdrawal of electrolyte ions seem to reduce the resistance. LR-700 anode containing the longitudinal channels as shown in Fig. 1 exhibits much lower resistance than P25 based on the measured overall impedances. The spherical TiO_2 nanoparticles of P25 have a large difference between the theoretical capacity and the actual capacity due to the limitation of the surface area to be reacted. However, the longitudinal channels of LR-700 allowed many areas to be used and reacted. Although the equivalent circuit model of LR-700 was slightly differently built compared to LTO, the overall impedances are very similar each other. On the other hand, P25 anode showed a very high overall impedance. These impedance data are well correlated to the performance of the three TiO_2 anodes.

Table 3. Comparison of the fitting parameters for EIS curves

	LR-700	LTO	P25
R_s (Ω)	3.83	3.12	2.47
R_{sf} (Ω)	9.26	-	50.33
R_{ct} (Ω)	5.87	15.02	495.2

CONCLUSION

Lotus-root shaped meso-/macroporous TiO_2 (LR-700) was fabricated using a CTAOH template and applied to the anode of LIBs. We prepared LIBs with P25 nano-sized TiO_2 having different particular characteristics as a comparative group and LTO as well for a reference sample. The electrical performance measurements showed that LR-700 has much higher capacity of 158 mAh/g even after the 50^{th} cycle, compared to 45 mAh/g of P25, probably because of its hierarchical longitudinal macroporous channels containing mesopores to make the supply and withdrawal of electrolyte easy. Although the surface area of P25 is two-fold larger than that of LR-700, too small pores of P25 might prevent the electrolyte from diffusing into the interior effectively. The capacity of LR-700 is also comparable to LTO (160 mAh/g) and the operating voltage of LR-700 is higher than LTO. The longitudinal macroporous channels of LR-700 play the role of passage for fast Li^+ migration, also supported by EIS measurements. However, the rate performance of LR-700 was slightly worse than LTO. Therefore, efforts to enhance the rate capability are needed in the future.

ACKNOWLEDGEMENTS

This work was supported by the Basic Science Research Program of the National Research Foundation of Korea (NRF), funded

by the Ministry of Education, Science and Technology (2019R1 I1A3A01040476, 2022R1F1A1063615). This work was also supported by the Hankuk University of Foreign Studies Research Fund of 2022 and the BB21plus funded by Busan Metropolitan City and Busan Institute for Talent & Lifelong Education (BIT).

REFERENCES

1. Y. Liu, G. Zhou, K. Liu and Y. Cui, *Acc. Chem. Res.*, **50**, 2895 (2017).
2. C. Zhu, R. E. Usiskin, Y. Yu and J. Maier, *Science*, **358**, eaao2808 (2017).
3. Y. Tang, Y. Zhang, W. Li, B. Ma and X. Chen, *Chem. Soc. Rev.*, **44**, 5926 (2015).
4. H. Kim, B. Han, J. Choo and J. Cho, *Angew. Chem. Int. Ed.*, **47**, 10151 (2008).
5. H. Kim, M. Seo, M.-H. Park and J. Cho, *Angew. Chem. Int. Ed.*, **49**, 2146 (2010).
6. W.-J. Zhang, *J. Power Sources*, **196**, 13 (2011).
7. J. R. Szczech and S. Jin, *Energy Environ. Sci.*, **4**, 56 (2011).
8. H. Lee, S. Choi, S. Choi, H.-J. Kim, Y. Choi, S. Yoon and J.-J. Cho, *Electrochem. Commun.*, **9**, 801 (2007).
9. C. Natarajan, K. Setoguchi and G. Nogami, *Electrochim. Acta*, **43**, 3371 (1998).
10. S. Y. Huang, L. Kavan, I. Exnar and M. Grätzel, *J. Electrochem. Soc.*, **142**, L142 (1995).
11. G.-N. Zhu, Y.-G. Wang and Y.-Y. Xia, *Energy Environ. Sci.*, **5**, 6652 (2012).
12. S. Scharner, W. Weppner and P. Schmid-Beurmann, *J. Electrochem. Soc.*, **146**, 857 (1999).
13. R. Fu, X. Zhou, H. Fan, D. Blaisdell, A. Jagadale, X. Zhang and R. Xiong, *Energies*, **10**, 2174 (2017).
14. J.-Y. Shin, D. Samuelis and J. Maier, *Adv. Funct. Mater.*, **21**, 3464 (2011).
15. F. Di Lupo, A. Tuel, V. Mendez, C. Francia, G. Meligrana, S. Bodoardo and C. Gerbaldi, *Acta Mater.*, **69**, 60 (2014).
16. T. Fröschl, U. Hörmann, P. Kubiak, G. Kučerová, M. Pfanzelt, C. K. Weiss, R. J. Behm, N. Hüsing, U. Kaiser, K. Landfesterd and M. Wohlfahrt-Mehrens, *Chem. Soc. Rev.*, **41**, 5313 (2012).
17. M. E. Davis, *Nature*, **417**, 813 (2002).
18. T. Ding, J. Wu, Z. Chen, T. Lan and M. Wei, *J. Electroanal. Chem.*, **818**, 1 (2018).
19. J. Li, J. Guo, J. Deng and Y. Huang, *Mater. Lett.*, **189**, 188 (2017).
20. Y. Li, X. Yan, W. Yan, X. Lai, N. Li, Y. Chi, Y. Wei and X. Li, *Chem. Eng. J.*, **232**, 356 (2013).
21. M. Zhen, X. Zhen and L. Liu, *Mater. Lett.*, **193**, 150 (2017).
22. Y.-G. Guo, Y.-S. Hu and J. Maier, *Chem. Commun.*, **26**, 2783 (2006).
23. S. Nagpure, Q. Zhang, M. A. Khan, S. Z. Islam, J. Xu, J. Strzalka, Y.-T. Cheng, B. L. Knutson and S. E. Rankin, *Adv. Funct. Mater.*, **28**, 1801849 (2018).
24. J. S. Chen and X. W. Lou, *Electrochem. Commun.*, **11**, 2332 (2009).
25. S. Ding, J. S. Chen, Z. Wang, Y. L. Cheah, S. Madhavi, X. Hu and X. W. Lou, *J. Mater. Chem.*, **21**, 1677 (2011).
26. F. Wu, Z. Wang, X. Li and H. Guo, *Ceram. Int.*, **40**, 16805 (2014).
27. K. Zhu, X. Liu, J. Du, J. Tian, Y. Wang, S. Liu and Z. Shan, *J. Mater. Chem. A*, **3**, 6455 (2015).
28. J.-Y. Hong, S.-E. Bae, Y. S. Won and S. Huh, *J. Colloid Interface Sci.*, **448**, 467 (2015).
29. J. Li, T. Zhang, C. Han, H. Li, R. Shi, J. Tong and B. Li, *J. Mater. Chem. A*, **7**, 455 (2019).
30. T. Ohzuku, A. Ueda and N. Yamamoto, *J. Electrochem. Soc.*, **142**, 1431 (1995).
31. D. Deng, M. G. Kim, J. Y. Lee and J. Cho, *Energy Environ. Sci.*, **2**, 818 (2009).
32. C. Han, Y.-B. He, S. Wang, C. Wang, H. Du, X. Qin, Z. Lin, B. Li and F. Kang, *ACS Appl. Mater. Interfaces*, **8**, 18788 (2016).
33. D. Aurbach, *J. Power Sources*, **89**, 206 (2000).
34. A. R. C. Bredar, A. L. Chown, A. R. Burton and B. H. Farnum, *ACS Appl. Energy Mater.*, **3**, 66 (2020).
35. J. Sastre, X. Chen, A. Aribia, A. N. Tiwari and Y. E. Romanyuk, *ACS Appl. Mater. Interfaces*, **12**, 36196 (2020).
36. L. Tang, Y.-B. He, C. Wang, S. Wang, M. Wagemaker, B. Li, Q.-H. Yang and F. Kang, *Adv. Sci.*, **4**, 1600311 (2017).
37. N. Sharma, J. Plévert, G. V. Subba Rao, B. V. R. Chowdari and T. J. White, *Chem. Mater.* **17**, 4700 (2005).